

# A simple, versatile method for GFP-based super-resolution microscopy via nanobodies

Jonas Ries, Charlotte Kaplan, Evgenia Platonova, Hadi Eghlidi & Helge Ewers

**We developed a method to use any GFP-tagged construct in single-molecule super-resolution microscopy. By targeting GFP with small, high-affinity antibodies coupled to organic dyes, we achieved nanometer spatial resolution and minimal linkage error when analyzing microtubules, living neurons and yeast cells. We show that in combination with libraries encoding GFP-tagged proteins, virtually any known protein can immediately be used in super-resolution microscopy and that simplified labeling schemes allow high-throughput super-resolution imaging.**

The single-molecule localization-based super-resolution imaging techniques such as photoactivated localization microscopy (PALM) and stochastic optical reconstruction microscopy<sup>1–4</sup> (here referred to as ‘single-molecule nanoscopy’) require specific and efficient delivery of bright fluorophores into close proximity of the target structure without adding substantial background. Present labeling techniques usually involve a tradeoff between these properties. Bright organic dyes can be delivered via antibodies, but their large size displaces the dye from the target in a ‘linkage error’ of ~10 nm, and highly specific antibodies are available only for some proteins. Methods based on photoactivatable fluorescent proteins or enzymatic labeling schemes demand the generation of new fusion constructs, which should be characterized and may not be functional.

We demonstrate a simple, efficient and versatile method that optimizes several labeling parameters and can be used with any of the thousands of functionally tested GFP constructs available. We used very small and high-affinity camelid antibodies (nanobodies) to GFP<sup>5</sup> to deliver bright organic fluorophores to GFP-tagged proteins for use in single-molecule nanoscopy.

Organic dyes are conventionally delivered to target structures via antibodies, which are ~150 kDa, ~10 nm in size and of varying affinity. In contrast, the 13-kDa anti-GFP nanobodies are smaller (1.5 nm × 2.5 nm) and have a high affinity for GFP (0.59 nM; ref. 5; **Supplementary Fig. 1**) and several of its

isoforms. Nanobody-mediated targeting of organic dyes to GFP-fusion constructs would combine the molecular specificity of genetic tagging with the high photon yield of organic dyes and minimal linkage error.

We covalently coupled anti-GFP nanobodies to Alexa Fluor 647 (AF647) and added them to MDCK cells expressing GFP anchored via glycosylphosphatidylinositol to the plasma membrane (GPI-GFP). The nanobodies bound to transfected cells readily at low concentrations but did not bind to untransfected cells (**Supplementary Fig. 1**). Labeled nanobodies exhibited highly specific and saturable binding at about 0.6 nanobodies per GFP (Online Methods).

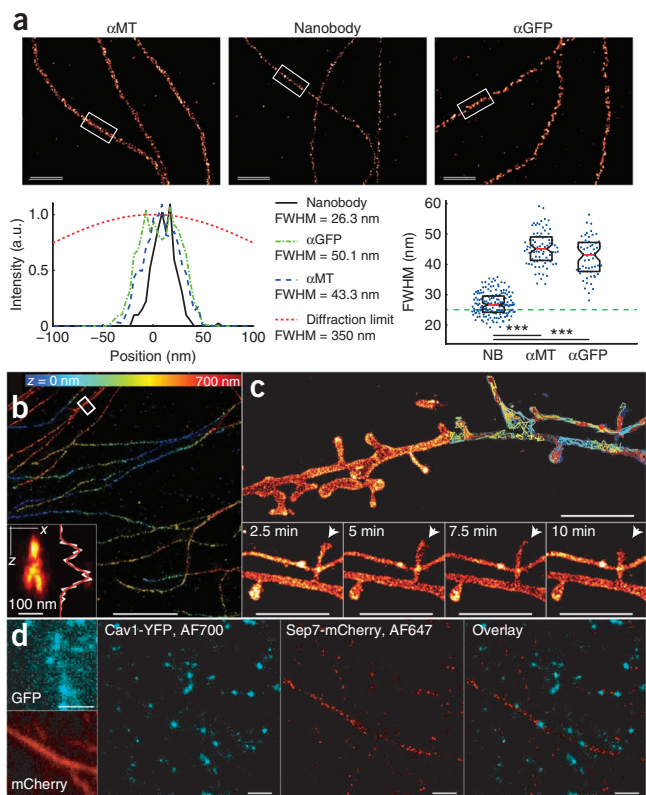
Under specific buffer conditions, many organic dyes become photoswitchable<sup>6,7</sup>. This fact is the basis for several single-molecule nanoscopy approaches<sup>2–4</sup>. To compare the nanobody-based approach to established methods, we labeled microtubules in fixed Ptk2 cells that stably expressed tubulin-YFP with AF647-anti-GFP nanobodies and imaged these cells by single-molecule nanoscopy. Individual microtubules were densely labeled with a full-width half maximum (FWHM) of 26.9 nm ± 3.7 nm (s.d.) (**Fig. 1a**), compatible with a microtubule diameter of 25 nm. This was significantly less (**Fig. 1a**) than what we achieved in parallel experiments using AF647-coupled secondary antibodies to detect microtubules either via anti-GFP (42.7 nm ± 7.0 nm) or anti-tubulin (45.6 nm ± 5.8 nm) antibodies, suggesting that the use of nanobodies led to minimal linkage error.

We next used the bright AF647-anti-GFP nanobodies for three-dimensional single-molecule nanoscopy with the bi-plane method<sup>8</sup>, which requires thousands of detected photons for good axial resolution. Nanobody-mediated labeling of microtubules in Ptk2 cells allowed us to resolve crossing microtubules with an axial separation of ~100 nm (**Fig. 1b**).

The use of bright labels not only increased localization precision (statistics in **Supplementary Fig. 2**), but also allowed the high frame rates required for imaging dynamic (live) samples. To realize this advantage, we transiently expressed GPI-GFP in primary hippocampal rat neurons and detected it via AF647-anti-GFP nanobodies. Single-particle tracking PALM (sptPALM)<sup>9</sup> allowed us to follow the trajectories of hundreds of molecules in the neuronal plasma membrane. We assembled a time series of super-resolution images and detected dynamic changes in the neuronal morphology over time (**Fig. 1c**).

Next, we used nanobodies for dual-color imaging. We realized this approach by using anti-GFP nanobodies labeled with Alexa Fluor 700 (AF700) and anti-RFP nanobodies (that also recognize monomeric (m)Cherry) labeled with AF647. We then labeled CV-1 cells expressing Septin7-mCherry and Caveolin1-YFP with these labels and could image both structures with high resolution and specificity (**Fig. 1d**).

**Figure 1 | Single-molecule nanoscopy by detection of GFP via nanobodies.** (a) Reconstructed super-resolution images obtained using different labeling strategies for microtubules in fixed Ptk2 cells stably expressing tubulin-YFP.  $\alpha$ MT, mouse anti-tubulin antibody plus secondary anti-mouse antibody labeled with AF647; nanobody, anti-GFP nanobody labeled with AF647; and  $\alpha$ GFP, mouse anti-GFP antibody plus secondary anti-mouse antibody labeled with AF647. Intensity profiles of microtubules were calculated from regions as indicated in the reconstructed super-resolution images, and the FWHM was determined by fitting with a Gaussian. Measured FWHM of microtubules from at least 60 line segments and three samples per labeling method. Boxes denote median values  $\pm$  quartiles, (\*\*\*, NB versus MT:  $P = 3.8 \times 10^{-52}$ ; and NB versus GFP:  $P = 2.7 \times 10^{-25}$ ; Mann-Whitney-test). Green dashed line indicates microtubule diameter. (b) Three-dimensional single-molecule nanoscopy of microtubules labeled with AF647-anti-GFP nanobodies. Inset, reconstructed  $x$ - $z$  image and  $z$  profile of a microtubule bundle denoted by the box. Distance between the peaks was 110 nm. FWHM of the top peak was 87 nm. (c) Live-cell super-resolution microscopy of cultured hippocampal neurons expressing GPI-GFP, labeled with AF647-anti-GFP nanobodies. Overlaid on the cumulative super-resolution image are single-molecule tracks obtained with sptPALM. Individual frames from super-resolution time-lapse imaging are shown. Arrows, areas with nanometer-scale morphological changes. For each time point subsets of 10,000 frames were used for reconstruction. (d) Dual-color super-resolution microscopy of a CV-1 cell expressing Caveolin-YFP and Septin7-mCherry labeled with AF700-anti-GFP and AF647-anti-RFP nanobodies, respectively. Scale bars, 2  $\mu$ m (single line) and 500 nm (double line) unless labeled otherwise.



Our labeling scheme made possible single-molecule nanoscopy of any GFP-tagged construct with minimal effort and hence could allow for high-throughput super-resolution imaging from libraries encoding GFP-tagged proteins (GFP-fusion libraries). To test this

possibility, we used a haploid *Saccharomyces cerevisiae* genomic library that encodes GFP-tagged proteins under the endogenous promoters<sup>10</sup> and developed a simple labeling scheme for AF647-anti-GFP nanobodies.

Yeast cells are generally immunostained after digestion of the cell wall, which generates spheroblasts and compromises cellular morphology. As this may affect the organization and localization of intracellular structures and is labor-intensive, we

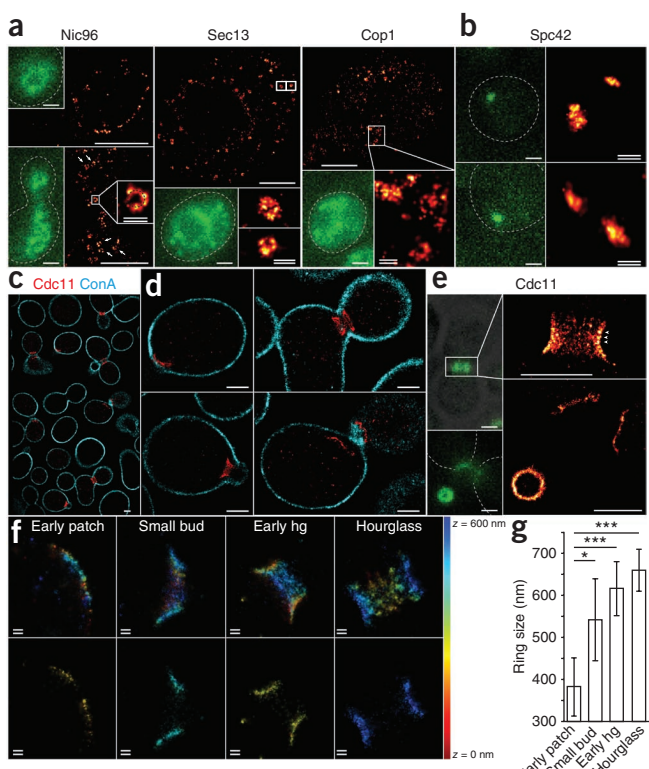


**Figure 2 | Single-molecule nanoscopy of proteins from a budding yeast GFP-fusion construct library.** (a) Reconstructed super-resolution images of Nic96-GFP, Sec13-GFP and Cop1-GFP. (b) Super-resolution images of the spindle pole body protein Spc42-GFP. (c) Dual-color reconstructed super-resolution images of a population of yeast cells expressing Cdc11-GFP stained with AF647-anti-GFP nanobodies (red) and the cell wall labeled with AF700-ConA (cyan). (d) Reconstructed dual-color super-resolution images visualizing the different organizational stages of Cdc11-GFP structures during the cell cycle. (e) Reconstructed super-resolution images of the yeast septin Cdc11-GFP, which localizes to a characteristic hourglass-shaped and later ring-like structure around the mother-bud neck. Dot-like structures are marked by arrowheads. (f) Reconstructed three-dimensional super-resolution images of the development of the bud-neck yeast septin structure over time. The central opening is visible in 200-nm-thick  $z$ -dimension sections. Hg, hourglass. Depth is color-coded from 0 to 600 nm. In a,b,e conventional wide-field images of the GFP fluorescence are shown in green. Owing to lack of optical sectioning, these wide-field fluorescence images might show higher background and lower contrast than state-of-the-art confocal or deconvoluted images. Scale bars, 1  $\mu$ m (single line) and 100 nm (double line). (g) Quantification of the diameter of the opening of the septin structure in the indicated stages ( $n = 9, 36, 20$  and  $18$  images analyzed for early patch, small bud, early hourglass (hg) and hourglass, respectively; error bars, s.d.; \* $P = 3.4 \times 10^{-5}$ , \*\*\* $P = 5.4 \times 10^{-7}$  (early patch versus hg),  $P = 1.5 \times 10^{-7}$  (early patch versus hg), Mann-Whitney test).

hypothesized that the small nanobodies might penetrate the cell wall of fixed, intact yeast cells after membrane permeabilization and developed a simple labeling scheme that would not require such a treatment.

As proof of principle, we analyzed structures of ~100 nm in size whose features are known, but have not been resolved by fluorescence microscopy so far, such as nuclear pores or coated vesicles. When we incubated fixed and permeabilized cells expressing GFP-tagged proteins in such structures with AF647-anti-GFP nanobodies and imaged them by single-molecule nanoscopy, we found that the nuclear pore complex component Nic96 localized to ring-like structures of ~70 nm diameter (**Fig. 2a**). When we imaged the COPII subunit Sec13, which forms cargo vesicles between the endoplasmic reticulum and the Golgi apparatus, we observed ring-like structures with diameters around 90 nm. The coatomer Cop1 yielded similar structures. To verify the suitability of our technique as a high-throughput method, we labeled another 20 GFP-tagged proteins from the library and performed single-molecule nanoscopy (**Supplementary Fig. 3**). Of these, the spindle pole body protein Spc42, which localizes to one diffraction-limited spot in the GFP channel, could be resolved to an elongated structure of  $108\text{ nm} \pm 20\text{ nm}$  length (**Fig. 2b**). In an analysis of 80 cells, we often (in 25 cells) found two structures about  $115\text{ nm} \pm 32\text{ nm}$  apart in the diffraction-limited spot. One of the structures usually appeared larger, suggesting the formation of a second spindle pole body (**Supplementary Fig. 4**).

Next we investigated the septin Cdc11-GFP, a molecule important in cell division<sup>11</sup> in more detail. When we incubated fixed and permeabilized cells with AF647 anti-GFP nanobodies and labeled the cell wall with the lectin concanavalin A coupled to AF700 (ConA-AF700), we could image both the cell wall and the septin structure in dual-color single-molecule nanoscopy<sup>12</sup> (**Fig. 2c**). We visualized the different organizational states of Cdc11-GFP-labeled structures during the cell cycle (**Fig. 2d**). During the hourglass structural state, we could resolve Cdc11-labeled point-like structures along the bud neck that resembled lateral cuts through periodic filaments (**Fig. 2e**; 13 of 21 structures investigated) in agreement with earlier observations using electron microscopy<sup>13</sup>.

How this septin ring is first assembled at the future bud site is unclear but it may involve a patch of septins<sup>14</sup> or a ring<sup>15</sup>. The resolution of conventional microscopy does not allow a quantitative investigation of this structure. When we synchronized cells and imaged them by single-molecule nanoscopy at different time points after release, we consistently observed holes in the center of even the earliest Cdc11 patches that increased in diameter with time (**Supplementary Fig. 5**). We then classified the structures according to their progression during the cell cycle (**Fig. 2f**) and quantified the size of the central opening. In the first structures (early patch) we observed, the central opening was  $382\text{ nm} \pm 70\text{ nm}$  ( $n = 9$ ) in diameter and this widened for hourglass structures to  $659\text{ nm} \pm 50\text{ nm}$  ( $n = 18$ , **Fig. 2g**). We concluded that nanobody labeling allows quantitative analysis of previously inaccessible structures in this important model organism.

We demonstrated here a simple, robust and versatile labeling scheme that enables the immediate use of any GFP-tagged molecule in yeast, tissue culture or neurons in single-molecule nanoscopy. Similar approaches combining GFP-tagging with

nanobodies may be generally useful for fluorescence microscopy and other applications such as immuno-electron microscopy or single-particle tracking. The small size and high affinity of the nanobodies allows for specific labeling in regions that are inaccessible to antibodies. Furthermore, compared with antibodies, the consistent affinity of nanobodies to GFP may allow for more comparable and quantitative labeling between different molecules. Although nanobodies have several advantages, in principle, the presented approach could also be realized using Fab fragments of anti-GFP antibodies. Our technique would be especially powerful in combination with the many available GFP knock-in mice.

GFP-tagged genomic libraries exist for several organisms, and our simple labeling protocol opens the door to high-throughput localization-analysis of entire proteomes at the nanoscopic level. Especially appealing is the yeast GFP-fusion library demonstrated here, as the constructs are expressed from the endogenous promoter in haploid strains. As a result, all molecules of a given protein are GFP-tagged, and our approach may allow for quantitative super-resolution microscopy in yeast cells and detection of molecules that are expressed in very low amounts.

## METHODS

Methods and any associated references are available in the online version of the paper.

*Note: Supplementary information is available in the online version of the paper.*

## ACKNOWLEDGMENTS

This work was supported by a Marie Curie Intra-European Fellowship (J.R.) the National Center for Competence in Biomedical Imaging and the National Center for Competence in Research ‘Neural Plasticity and Repair’. We thank Y. Barral and members of the Barral laboratory for useful discussions, help with yeast strains and access to the yeast genomic GFP-fusion library, R. Dechant for help with elutriation and M. Stoeber for help with Amaxa transfection.

## AUTHOR CONTRIBUTIONS

H. Ewers conceived of the project; J.R., C.K., E.P. and H. Ewers designed experiments; J.R., C.K., E.P., H. Eghlidi & H. Ewers performed and analyzed experiments; H. Ewers and J.R. wrote the paper.

## COMPETING FINANCIAL INTERESTS

The authors declare no competing financial interests.

Published online at <http://www.nature.com/doifinder/10.1038/nmeth.1991>. Reprints and permissions information is available online at <http://www.nature.com/reprints/index.html>.

1. Betzig, E. et al. *Science* **313**, 1642–1645 (2006).
2. Rust, M.J., Bates, M. & Zhuang, X. *Nat. Methods* **3**, 793–795 (2006).
3. Heilemann, M. et al. *Angew. Chem. Int. Edn. Engl.* **47**, 6172–6176 (2008).
4. Fölling, J. et al. *Nat. Methods* **5**, 943–945 (2008).
5. Rothbauer, U. et al. *Nat. Methods* **3**, 887–889 (2006).
6. Bates, M., Blosser, T.R. & Zhuang, X. *Phys. Rev. Lett.* **94**, 108101 (2005).
7. Heilemann, M., Margeat, E., Kasper, R., Sauer, M. & Tinnefeld, P. *J. Am. Chem. Soc.* **127**, 3801–3806 (2005).
8. Juette, M.F. et al. *Nat. Methods* **5**, 527–529 (2008).
9. Manley, S. et al. *Nat. Methods* **5**, 155–157 (2008).
10. Huh, W.-K. et al. *Nature* **425**, 686–691 (2003).
11. Hartwell, L.H. *Exp. Cell Res.* **69**, 265–276 (1971).
12. Baddeley, D. et al. *PLoS ONE* **6**, e20645 (2011).
13. Byers, B. & Goetsch, L. *J. Cell Biol.* **69**, 717–721 (1976).
14. Cid, V.J., Adamková, L., Sánchez, M., Molina, M. & Nombela, C. *Microbiology* **147**, 1437–1450 (2001).
15. Chen, H., Howell, A.S., Robeson, A. & Lew, D.J. *Biol. Chem.* **392**, 689–697 (2011).

## ONLINE METHODS

**Cell culture.** Ptk2 cells stably expressing tubulin-YFP were maintained in phenol-red free DMEM (Invitrogen) supplemented with 10% FCS (Labforce), Glutamax (Invitrogen) and 500 µg/ml G418 (Invitrogen). Cells were plated on 18 mm round coverglass and after 24 h were permeabilized for 5 min at 37 °C in 0.25% Triton X-100 in BRB80 (80 mM PIPES, 1 mM MgCl<sub>2</sub> and 1 mM EGTA, pH 6.8). They were then fixed in methanol at -20 °C and washed in BRB80. Cells were blocked in BRB80 with 1% BSA and 4% horse serum and incubated for 30 min with 250 ng/ml AF647-labeled nanobodies. Buffer for single-molecule nanoscopy measurements in Ptk2 cells is based on that in ref. 3: 150 mM Tris-HCl, 60 mM β-mercaptoethylamine (Sigma), 1% v/w glucose, 0.5 mg/ml glucose oxidase (Sigma) and 40 µg/ml catalase (Sigma).

**Neuronal cell culture.** Cultures of hippocampal neurons were from E18 Sprague-Dawley rats. Embryos were removed and placed in ice-cold HBSS, decapitated and brains put into a new dish containing ice-cold HBSS. Both cerebral hemispheres were removed and freed from their meninges. The hippocampi were dissected and collected in fresh HBSS. After 15 min incubation in prewarmed trypsin (Invitrogen), neurons were singularized by pipetting up and down in a 1,000-µl pipette tip, plated at a density of 2–3 × 10<sup>5</sup> cells/dish on poly(lysine)-precoated cover slips and kept in neurobasal medium (Invitrogen) at 37 °C in 5% CO<sub>2</sub>. After 3 d, cytarabine was added to 5 µM. Neurons were transfected using Lipofectamine (Life Technologies) as described previously<sup>16</sup>. All live cell microscopy was performed in extracellular solution (ECS; 145 mM NaCl, 5 mM KCl, 2 mM CaCl<sub>2</sub>, 1 mM MgCl<sub>2</sub>, 10 mM HEPES and 10 mM glucose) supplemented with 0.2% bovine serum albumin at pH 7.4, and osmolarity was adjusted to that of the cellular medium. For single-molecule nanoscopy measurements, the solution was supplemented with 200 mM HEPES, 30 mM β-mercaptoethylamine (MEA), 0.5% (v/w) glucose, 0.25 mg/ml glucose-oxidase and 20 µg/ml catalase.

**Poly(lysine)-coating of coverglass.** Coverslips were incubated overnight in HNO<sub>3</sub>, washed six times in ddH<sub>2</sub>O and dried overnight in an oven at 250 °C. Four coverslips were placed in 6-cm dishes and coated with 200 µl of 1 mg/ml poly(lysine) solution (MW 30,000–70,000, Sigma), incubated for 3 h at 37 °C and afterwards washed three times in ddH<sub>2</sub>O.

**Preparation of yeast strains for single-molecule nanoscopy.** Standard methods and media were used to cultivate yeast cells<sup>17</sup>. Yeast strains are listed below.

Overnight cultures were diluted to OD 0.2 in 5 ml of yeast rich medium (yeast extract peptone dextrose; YPD) in a 50 ml Falcon tube and grown for 3 h at 30 °C. Cells were spun down for 4 min at 2,800 g and resuspended in 200 µl ddH<sub>2</sub>O. A 50 µl drop of cell suspension was pipetted onto concanavalin A-coated coverglass. The suspension was allowed to settle down for 15 min, remaining liquid was taken away and cells were fixed for 15 min in 4% paraformaldehyde (PFA), 2% sucrose in phosphate-buffered saline (PBS). The fixation was stopped by two washes for 15 min in PBS with 50 mM NH<sub>4</sub>Cl.

Subsequently, cells were blocked and permeabilized by gently shaking for 30 min in PBS with 0.25% Triton X-100, 5% BSA and 0.004% NaN<sub>3</sub> in 1× PBS. After blocking, the cells were labeled for 90 min in 100 µl of nanobody solution (10 µM labeled nanobody,

0.25% Triton X-100, 1% BSA and 0.004% NaN<sub>3</sub> in 1× PBS). Cells were then washed for 5 min by gently shaking in PBS. Depending on the quality of the staining, more washing steps were performed before mounting the cover slip onto the sample holder. Buffer for localization microscopy was the same as for Ptk2 cells. For Tub1 staining, in all steps BRB80 buffer was used instead of PBS.

**Dual-color labeling of yeast cells for single-molecule nanoscopy.** For dual-color labeling of yeast cells, coverslips were washed one time after the nanobody labeling step for 5 min in 1× PBS. The ConA-labeled with AF700 was diluted to 70 nM in a solution containing 1% BSA and 0.04% NaN<sub>3</sub> in PBS. Coverslips were transferred onto Parafilm again and incubated for 30 min in 100 µl secondary staining solution. Subsequent washing steps were performed as mentioned above.

**Dual-color labeling with nanobodies.** For dual color labeling of mammalian cells, cells were washed three times with BRB80, fixed in 4% PFA in BRB80 for 15 min at room temperature. Coverslips were then incubated for 15 min in BRB80 with 50 mM NH<sub>4</sub>Cl and then permeabilized in BRB80 with 0.25% Triton-X100 for 5 min. Cells were washed three times for 5 min in BRB80 and then incubated for 30 min in 4 drops of Image-it FX (Invitrogen). Cells were blocked for 45 min in BRB80 with 1% BSA and 4% horse serum and then labeled with 50 ng/ml of AF647-anti-RFP and AF700-anti-GFP nanobodies. Buffer for localization measurements was 150 mM Tris-HCl pH 8.8, 1.5% β-mercaptoethanol, 0.5% (v/w) glucose, 0.25 mg/ml glucose oxidase and 20 µg/ml catalase.

**Preparation of concanavalin A coverglass.** Round 18-mm-diameter cover slips (Assistent) were placed in a Petri dish with ddH<sub>2</sub>O and washed twice with ddH<sub>2</sub>O. Then they were submerged in 70% ethanol for at least 5 min. The required amount of cover-glass was air-dried and placed on Parafilm. A 20-µl drop of a 2 mg/ml concanavalin A solution (ConA, C7275, Sigma-Aldrich) was distributed onto each cover slip and spread with a pipette tip to cover it completely. The coverglass was left at room temperature to let the ConA attach and after 30 min the rest of the ConA solution was taken away. To dry the ConA completely, the glass was incubated for 1 h at 37 °C.

**Synchronization of yeast cells.** Cell-cycle synchronization was performed with a JE-5.0 elutriation rotor in an Avanti-J20 XP centrifuge (Beckmann). A 600-ml yeast culture was grown to OD = 1 for 3 h at 30 °C and was flooded into the funnel-shaped chamber of the rotor with a starting flow rate of 18 ml/min and a centrifuge speed of 2,000 r.p.m. As the chamber filled up with cells, the flow rate and centrifuge speed were adjusted to establish a sharp border in between the differently sized cells as monitored through the observation window. Cells were finally separated in the flow chamber at a flow rate of 6 ml/min and 3,000 r.p.m. The G1 fraction was collected with an initial flow rate of 11 ml/min that increased to 13 ml/min at the end. Homogeneity of the fraction was controlled by microscopy of cell samples.

We collected 300 ml of synchronized G1 cells and immediately concentrated them by filtering. Cells were resuspended in 50 ml YPD medium and incubated at 30 °C on a shaker (120 r.p.m.). Seven milliliters of yeast culture was fixed in a ratio 1:1 with 8% paraformaldehyde and 4% sucrose in 1× PBS at time points 0 min,

2 min, 5 min, 10 min, 15 min and 25 min. Fixation was performed for 15 min at room temperature, cells were washed once in 3 ml PBS with 50 mM NH<sub>4</sub>Cl by gently shaking for 30 min and then stored in 1× PBS at 4 °C. Mounting and staining was performed as described in the protocol above.

**Preparation of labeled nanobodies.** Nanobodies were purchased from Chromotek as GFP-Trap and RFP-Trap. For labeling, 50 µl of the 1 mg/ml solution were dialyzed into 0.2 M NaHCO<sub>3</sub>, pH 8.2 in a mini-dialysis unit (Pierce, molecular weight cutoff = 3,500 Da). Succinimidyl-esters of Alexa Fluor 647 and Alexa Fluor 700 (Invitrogen) were dissolved at 10 mg/ml in DMSO, stored at –80 °C and for labeling added to fivefold molar excess to the nanobodies. The mixture was incubated for 1–2 h at 25 °C. Excess dye was removed via buffer exchange into PBS using Zeba desalting columns (Pierce, molecular weight cutoff = 7,000 Da), and the solution was stored at 4 °C.

**Preparation of labeled concanavalin A.** Concanavalin A was dissolved at 2 mg/ml in 0.2 M NaHCO<sub>3</sub>, pH 8.2 and incubated for 1 h with a fivefold molar excess of Alexa Fluor 700 succinimidyl-ester (Invitrogen). Excess dye was removed by a desalting column (Amersham).

**Optical setup.** Single-molecule nanoscopy was performed with a custom-built microscope. A 473 nm laser (100 mW) and a 647 nm laser (150 mW, both lasers from Pusch OptoTech) were mode-cleaned with a pinhole and focused onto the back-focal plane of a total internal reflection fluorescence (TIRF) objective (numerical aperture (NA) 1.49, 60×; Olympus) for highly inclined plane illumination. Emission light was filtered by a 700/75 and a 675/50 band pass (AHF) and focused by a 500 mm tubus lens onto the chip of a back-illuminated electron-multiplying charge-coupled device (EM-CCD) camera (Evolve, Photometrics) that was water-cooled to –85 °C. Images were acquired with MicroManager<sup>18</sup>.

For 3D localization, the emission was split by a nonpolarizing 50:50 beam splitter cube and focused by two tube lenses onto different parts of the camera. The position of the tube lenses was adjusted to result in a difference in focal planes of  $\Delta z = 400$  nm.

For dual-color imaging, two 700/75 nm band-pass filters were used. A dichroic (LP 690, AHF) split the emission into two channels, which were imaged onto two parts of the CCD chip.

Focusing was done by moving the objective with a piezo objective positioner (MIPOS, Piezo Systems Jena). A focus lock was implemented by an electronic feedback loop (LabView, National Instruments) based on the total internal reflection of a red laser at the cover slip and its detection by a quadrant photodiode; the  $z$  stability was better than  $\pm 10$  nm over several hours. The lateral drift was typically smaller than 50 nm/h; a drift-correction was implemented on the level of the analysis software (see below). For live-cell imaging, the temperature was stabilized to 35 °C with a proportional-integral controller by heating the bottom plate of the encapsulated microscope.

**Determination of labeling efficiencies.** The labeling efficiency of the nanobodies with Alexa Fluor dyes was determined by absorption spectroscopy after removing excessive dye two times

as described above. Typical labeling efficiencies were around  $\epsilon = 0.6$  AF647 molecules per nanobody.

Binding efficiencies of the nanobodies (NB) to GFP were determined in the following way. A mixture of GFP and AF647 in PBS, 1% BSA, 0.005% Tween was prepared and their concentrations C<sup>0</sup><sub>GFP</sub> and C<sup>0</sup><sub>AF647</sub> were measured by absorption spectroscopy. Calibration images in the AF647 and the GFP channel (I<sup>0</sup><sub>AF647</sub>, I<sup>0</sup><sub>GFP</sub>) on this solution were taken under conditions identical to the later measurements. Images of nanobody-labeled structures (MDCK cells expressing GPI-GFP) were normalized pixel-wise by the calibration images and low-pass filtered. The labeling ratio in each pixel was then determined according to: NB/GFP =  $(1/\epsilon)(I_{AF647}/I^0_{AF647})(I^0_{GFP}/I_{GFP})(C^0_{AF647}/C^0_{GFP})$ .

Labeling efficiencies were around 0.6 NB/GFP, both for labeling performed before and after fixation.

**Single-molecule measurements.** The samples were mounted in a custom-made holder, the measurement chamber was filled with 200 µl of the respective buffer, and the chamber was mounted on the microscope. We used an exposure time of 25 ms (15 ms for live-cell imaging) and an electron multiplier gain of 300. Imaging laser intensity at 642 nm was 5 kW/cm<sup>2</sup> (2.5 kW/cm<sup>2</sup> for live-cell imaging); the activation laser was automatically adjusted to keep the average number of localizations per frame constant (maximum intensity 0.25 kW/cm<sup>2</sup>). Typically 20,000–100,000 frames were acquired.

**Localization analysis.** Localization analysis was performed as described before<sup>19</sup>. Briefly, pixel counts were converted to photons by subtracting the constant offset and multiplying by the inverse gain. Approximate locations of bright spots in each image were determined by smoothing, nonmaximum suppression and thresholding. Selected regions of interest were fitted by a pixelized Gaussian function and a homogeneous photonic background with a maximum likelihood estimator (MLE) for Poisson distributed data using a freely available, fast GPU fitting routine<sup>20</sup> on a GeForce GTX275 (Nvidia). Lateral drift was corrected based on the imaged features: blocks of typically 5,000 frames were used to reconstruct one PALM image. Displacements among all reconstructed images were determined by image correlation and fitting of the maximum with an elliptical Gaussian. Displacements corresponding to each time point were averaged using a robust estimator, interpolated by a spline and used to correct the position of each localization. From the variation of the spline, we estimate that the residual error for the corrected positions was about 2 nm.

For fixed cells, localization bursts with a distance smaller than 90 nm in consecutive frames (interrupted by not more than two frames) were grouped into a single localization. Finally, localizations with an uncertainty of  $\sigma_{\max} > 10$  nm (15 nm for live-cell imaging) were discarded.

For 3D localization, the axial position of the fluorophores was inferred from the measured sizes  $\sigma_1$  and  $\sigma_2$  of the single-molecule images using a calibration with 40 nm fluorescent beads (TransFluoSpheres 488/645, Invitrogen). To this end, localizations in the two channels originating from one molecule had to be linked. This was achieved by calculating an approximate shift between the two channels by cross-correlating the images, linking the brightest molecules in each frame, which were then used to calculate an affine transformation between the two channels.

This transformation was used to map the positions of channel 2 onto channel 1. Finally, all molecules were linked and their axial position was calculated. Even higher axial localization precision can in principle be achieved by using an experimental PSF for data fitting<sup>21</sup> instead of a Gaussian.

For dual-color imaging, the transformation between the two channels was calculated using all AF647 localizations, which were visible in both channels. Subsequently, for each localization, background-corrected intensities from corresponding regions in the two channels were compared to assign the proper identity of the label.

For the images in **Figures 1** and **2**, the localization data were rendered using a Gaussian with a width according to the localization precision of the respective localization, determined from the fitted number of photons and background. Line profiles (**Fig. 1a**) were obtained by binning the localizations inside the selected region along the cross-section in intervals of 4 nm. The FWHM (**Fig. 1a,b**) was determined by fitting a Gaussian to the binned data. All analysis software was written in Matlab (Mathworks).

**Yeast strains and proteins.** All yeast strains were obtained from a yeast GFP-fusion library<sup>10</sup> (Invitrogen). In this study we investigated the localization of the yeast proteins Cdc11, Nic96, Bfr2, Spc42, Bud3, Pmp1, Rox3, Htx3, Sir2, Kar3, Nop2, Pma1, Tub1, Snf7, Cdc14, Cop1, Erg6, Sec13, Sur7, Tom20, Vma2, Nic96, Mep2, Hho1, Ilv6 and Fet3, which we selected for their distinct localization pattern according to ref. 6. Detailed information can be obtained from <http://www.yeastgenome.org/> and in the **Supplementary Note**.

16. Kaech, S. & Banker, G. *Nat. Protoc.* **1**, 2406–2415 (2006).
17. Amberg, D.C., Burke, D. & Strathern, J.N. *Methods in Yeast Genetics*. (Cold Spring Harbor Laboratory Press, 2005).
18. Edelstein, A., Amodaj, N., Hoover, K., Vale, R. & Stuurman, N. *Curr. Protoc. Mol. Biol.* **14**, 20 (2010).
19. Schoen, I., Ries, J., Klotzsch, E., Ewers, H. & Vogel, V. *Nano Lett.* **11**, 4008–4011 (2011).
20. Smith, C.S., Joseph, N., Rieger, B. & Lidke, K.A. *Nat. Methods* **7**, 373–375 (2010).
21. Juette, M.F. & Bewersdorf, J. *Nano Lett.* **10**, 4657–4663 (2010).